Journal of Magnetics 8(1), 60-69 (2003)

Magnetic Sensors and Actuators

M. Pasquale*

IEN Galileo Ferraris, Strada delle Cacce 91, 10135 Torino Italy

(Received 10 December 2002)

A review of mechanical sensing techniques based on magnetic methods is presented, with special reference to magnetoelastic strain gauges and force sensors. A novel strain sensor, based on soft amorphous ribbons is described. Other types of magnetic sensors, for the measurement of torque and displacement are briefly discussed. An overview of magnetic actuators based on giant magnetostrictive materials, with some practical examples, is presented. Recent advances in the development and application of magnetic shape memory materials are discussed, together with the analysis of recent studies for the description of magnetic shape memory phenomena.

1. Introduction

Mechanical sensors of mechanical quantities are used in a wide range of applications and only a limited number of categories will be discussed in this contribution. A sufficiently complete list of mechanical sensors can be found in the definition of the IEEE Sensors council field of interest. In this list we find: metallic, thin-film, thick film and bulk strain gauges; pressure sensors; accelerometers; angular rate sensors; displacement transducers; force sensors; bulk and surface acoustic wave sensors; ultrasonic sensors; flow meters and flow controllers. Wishing to limit the scope of this discussion, we choose sensors and transducers based on the direct or inverse magnetostrictive and magneto-elastic effects *i.e.* strain and force sensors; torque sensors; displacement sensors. Magnetostrictive actuation is particularly suitable to high force actuation, where large magnetic fields are required to achieve large strain coupled to large forces. A limited number of magnetostrictive actuators have been constructed, and only recently they have been mass produced. The number of magnetostrictive actuators is anyhow increasing, since smart design may lower the energy input requirements. In past few years a new class of magnetically activated shape memory materials, in the form of bulk single crystals has been recognized and studied. It has been found that the motion of the twin boundaries of the martensite phase driven by magnetic field may lead to a very large strain (up to 6%) at low load (<10 MPa). It is interesting to observe that the analysis of structural properties and the control of magnetic anisotropy lead to the successful applications of bulk magnetic (magnetostrictive and/or shape memory) materials to sensing and actuation. A proper control of the anisotropy is even more crucial in the case of thin magnetic films, due to the particularly strong interplay between the thermal and magneto-mechanical characteristics of the film and the thermal and mechanical properties of the substrate. In any case we should be aware that magnetic materials always have hysteretic characteristics, which may have to be taken into account in the design and operation of magnetostrictive as well as shape memory based transducers.

*Corresponding author: Tel: +39 011 391 9820; Fax: +39 011 3919834, e-mail: pasquale@ien.it

2. Issues in magnetic sensing and actuation

Magnetostriction, *i.e.* a deformation induced by an applied magnetic field, can be used to convert magnetic energy in a displacement, a typical example of actuation, while typical magnetic sensor applications rely on the inverse magnetostrictive effect, where the magnetic properties of the material are affected by the application of a mechanical load/stress. In both cases a detailed description of the magneto-mechanical behavior of a material is far from trivial, since magnetostrictive properties, which are related to the mechanical behavior of a material, are naturally described by a tensor quantities. To further complicate matters, both the mechanical and magneti-

zation behavior of materials are typically hysteretic processes which dissipate energy and where a multiplicity of states is available depending on past history. Given the intrinsic high complexity of the physics, we typically choose a practical approach, where some strong simplifications and assumptions must be made, to allow an acceptably simple description of the phenomena.

The magnetostrictive process relating the magnetic and mechanical material states can be roughly described with the two coupled linear equations. These equations neglect the effect of temperature and have been reduced to scalar form where the stress/strain and the applied field are collinear along the z direction. In the magnetostrictive equations of state several mechanical parameters appear (strain ε, stress σ, Young's modulus at constant field E_y^H), magnetic parameters (applied magnetic field H, magnetic induction B, permeability at constant stress μ^σ), and two magneto-mechanical coefficients (the axial strain coefficient $d_{33} = \partial\varepsilon/\partial H|_\sigma$, and its inverse $d_{33}^* = \partial B/\partial\sigma|_H$.

$$\varepsilon = \sigma/E_y^H + d_{33}H \quad \text{(a)}$$

$$B = d_{33}^*\sigma + \mu^\sigma H. \quad \text{(b)}$$

These equations should be considered just as a crude first approximation for analyzing the coupled mechanical and magnetic behavior of magnetostrictive materials. Equation a) shows that the strain of a magnetostrictive body changes with stress and applied magnetic field. When a stress σ is applied to a magnetostrictive sample, it will strain and the effect is inversely proportional to the elastic modulus E_y^H. An applied magnetic field H, can also change the sample's length and the effect of H is scaled by the piezomagnetic coefficient, d_{33}. The elastic modulus and the piezomagnetic coefficients vary from one magnetostrictive material to the next. Unfortunately, just as the $B = \mu H$ law, can be used as a very rough approximation of the magnetic behavior of a material, the above equations cannot take in to account the magnetic and mechanical non linearity and hysteresis phenomena, nonetheless they are a good starting point to analyze the behavior of a body with magnetostrictive properties.

3. Mechanical sensing techniques

According to equations a) and b) we can use a magnetostrictive material to convert a change in dimensions into an electric signal which can be further processed. Magnetostrictive sensors can be divided in passive or active sensors depending on the type of transduction used: a passive sensor may rely on the inverse magnetostriction to measure most mechanical quantities such as load/force/pressure and flow rates while active sensors may be used to obtain higher sensitivity or a linear behavior, just as in most magnetic field sensors based on the carrier technique or in the case of transformer type sensors.

4. Magnetoelastic strain gauges and force sensors

Many Fe, Ni or Co based magnetic materials in the form of thin-thick films, ribbons or bulk can be successfully employed as sensing elements for deformation. Many types of magnetic strain gauges can be constructed and the operating principle is based on inverse magnetostriction, where the dc or ac permeability changes are induced by an applied compressive or tensile stress (figure 1 and eqs. a, b). A clarifying example can be considered: an amorphous TbFe thin film shown in figure 1 has a large magnetostriction (up to $\lambda_s \approx 4 \times 10^{-4}$) and a rather strong in plane anisotropy in the zero applied stress state [1-4]. From the figure we can observe that in plane anisotropy increases with tensile stress and vanishes with coercivity and remanence when the stress is compressive, an indication of out-of-plane anisotropy being developed. These characteristics may be exploited for stress sensing using an excitation field and a pick up coil, where maximum permeability changes will appear as differences in the output peak voltages.

Magnetostrictive materials can be produced with values of positive or negative magnetostriction for specific applications by tuning composition, and proper magnetic conditions leading to linear magnetic conditions can be achieved by preparation or post processing through field/stress annealing, in order to induce the desired degree of anisotropy. As an example we can study the behavior

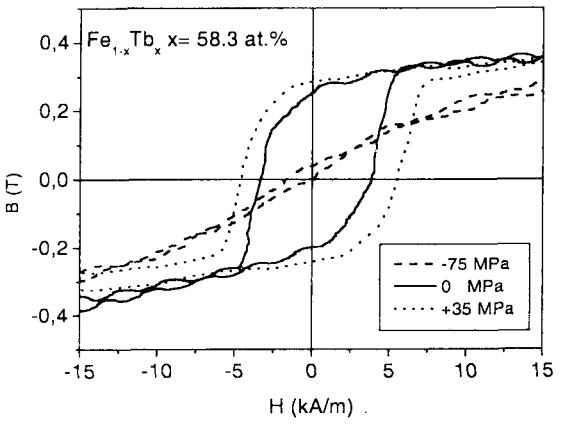

Fig. 1. Hysteresis loop of a 1 μm thick FeTb amorphous film on a 200 μm Si substrate under tensile and compressive stress. Magnetic permeability changes can be exploited for sensing applications.

under stress of an amorphous CoFeB alloy with a small negative magnetostriction to monitor the deformation of concrete structures under static or dynamic load. Magnetically softer amorphous ribbons (thickness < 30 μm), having a small coercive field and vanishing terms of anisotropy, are particularly sensitive to external stress and they can be excited at a few kHz without the detrimental influence of eddy current shielding. Once the ribbon is stress or field annealed it is possible to obtain a highly linear response of the permeability in a wide range of applied tensile or compressive stress/deformations, which in a reinforced concrete structure may reach $\sigma \approx 500$ MPa and $\varepsilon \approx 2 \times 10^{-3}$. Due to the particularly wide stress and deformation range a thin magnetic film on a rigid Si substrate does not couple well mechanically. We can otherwise exploit the fact that the reinforcement in concrete is made of steel and a CoFe based amorphous ribbon, will posses comparable mechanical characteristics. After a proper optimization with a stress annealing which induces a strong transversal anisotropy (figure 2 inset) we can achieve the desired linear magnetic behavior shown in Figure 2. The possibility of sensing a wide range of applied stress is due to the combination of tensile stress and small negative magnetostriction. It should be noted that this combination leads to an increase of the transversal anisotropy under tensile stress but does not lead to saturation of the sensor at practical levels of applied stress.

Both force sensors and strain gauges based on magnetostrictive ribbons or films can employ the change in electrical impedance of a coil wound around the magnetostrictive element to detect the mechanical load [5]. Several circuit configurations are possible with one or two

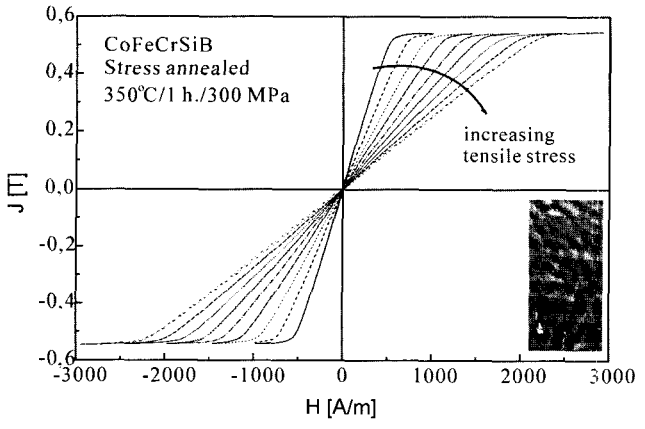

Fig. 2. Linear hysteresis loops measured at increasing levels of applied tensile stress on a stress annealed amorphous CoFe ribbon. Maximum tensile stress 350 MPa. Inset shows the transversal domain structure. Longitudinal sample direction up-down, photo dimensions 0.9 × 1.7 mm. Courtesy of F. Fendrich L. Kraus (CAS Prague).

coils. In a one coil circuit the force/strain may be detected as an inductance change of the RLC circuit containing the magnetostrictive element, measuring for instance the change in resonant frequency. In the case of a two coils circuit we can keep the primary coil current constant and detect changes in the output voltage from the secondary coil or better we can use a constant flux operating mode which is more sensitive to structural changes of the magnetostrictive material. In this type of measurement we modify the excitation current to maintain a constant detection coil output voltage. Comparing with conventional force transducers employing strain gauges, these force sensor are simpler, produce output voltage signals three orders of magnitude higher. Another possible configuration for force sensors relies on the changes of peak magnetization at a constant applied field. In ref. [8] a set of hysteresis loops is obtained by applying a sinusoidal magnetizing current to an amorphous magnetic core, and each loop is obtained with an increasing applied force. The method has a good linearity for low levels of applied stress (>1% deviation up to 2.5 MPa. It should be especially noted that in the case of magnetization close to technical saturation the hysteresis properties of the material have no direct influence on the measured quantity as the property studied is not influenced by the loop area.

5. Torque sensors

Just as in the case of force measurements we can use the inverse magnetostrictive effect to detect torque through the magnetization change induced in our sensor by a torsional stress. Torque measurements are useful in a great variety of applications such as rotating machines, high power engines but also in the automotive field where low torque measurements can be used for power steering. Several possible configurations can be used: the magnetization of the sensor can be measured directly (as a passive sensor), or after an excitation as a change in permeability or inductance in a coupled circuit [6]. In the case of slightly ferromagnetic shafts the magnetostrictive material can be bonded with several techniques (gluing, bonding, brazing, plasma spraying etc.), or if the shaft is reasonably ferromagnetic it can itself be employed for the measurement, after a proper magnetization. A possible configuration relies on one or two circularly magnetized rings. As a torque is applied to the shaft a magnetic field appears at in proximity of the region, directly proportional to the applied torsional stress. Two rings magnetized in opposite directions increase the output magnetic field signal see Figure 3 [9] which can be detected by Hall probes or other field sensors. An interesting example is

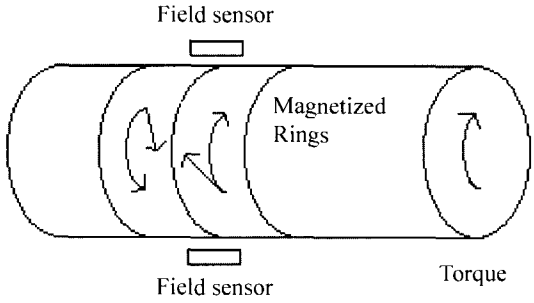

Fig. 3. Double ring torque transducer from [9]. Each ring is circularly magnetized in the opposite direction. Applied torque causes a rotation of the remanent magnetization of the circular direction.

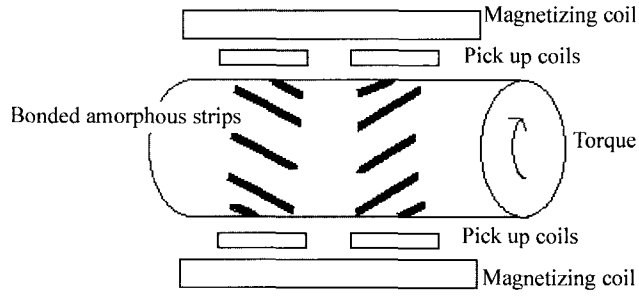

Fig. 4. Torque sensor on a non magnetic shaft from [10]. Negative magnetostrictive chevrons are attached with mirror symmetry and magnetized along the axis by a solenoid with a constant field. Differences in the magnetization of the chevrons due to torsional stress are measured by the pick up coils.

[7] the torque measurement on a drill bit: a coil surrounds a part of the drill including the shank and the flutes. Two series opposition coils, positioned one over the flutes and one over the shank, allow the measurement of the permeability. The permeability of the shank is less sensitive to changes in torque than the flutes and the difference in the output voltages of the two coils is proportional to the applied torque. Another possible configuration for torque measurements on a shaft relies on the difference in saturation magnetization of two regions of amorphous magnetic material, which are designed with a chevron geometry (see Figure 4 and ref. [10]). In the specific case a Co based, negative magnetostrictive ($\lambda_s \approx -6 \times 10^{-6}$) ribbon was used, cut in the shape of a chevron. Two patterns of magnetic chevrons are attached to the non magnetic shaft, with mirror symmetry. Due to the different geometry, the patterns, which are magnetized along the axis of the shaft by a solenoid with an applied constant current, are subject to a different reorientation of the magnetic anisotropy with the application of a variable torsional stress. In one pattern the material will be subjected to a predominantly compressive stress while the other pattern will be subjected to a tensile stress. This difference leads to an unbalanced magnetization which can be detected by the two pick up coils connected in series opposition [10].

6. Displacement sensors

Many magnetostrictive position sensors are constructed using a magnetostrictive wire (*i.e.* a Ni wire) and position sensing is obtained through the Wiedemann effect. The Wiedemann effect is a localized mechanical twisting due to the superposition of a circular field and a longitudinal field generated by two sources, respectively a) a current pulse propagating through the wire b) a longitudinal magnetic field produced by a permanent magnet at a certain position along the wire. The sensor can be built in this way: an electric pulse propagates from the source end toward the other wire end. As it the pulse and the connected circular field reaches the position of the permanent magnet a localized mechanical twisting occurs (the Wiedemann effect), and the mechanical wave starts propagating toward both wire ends at the proper speed of sound (in the range of 5000 m/s). Since the electric signal propagates at a much higher speed given by $1/\sqrt{\mu\varepsilon}$ the magnet position can be computed as the delay between

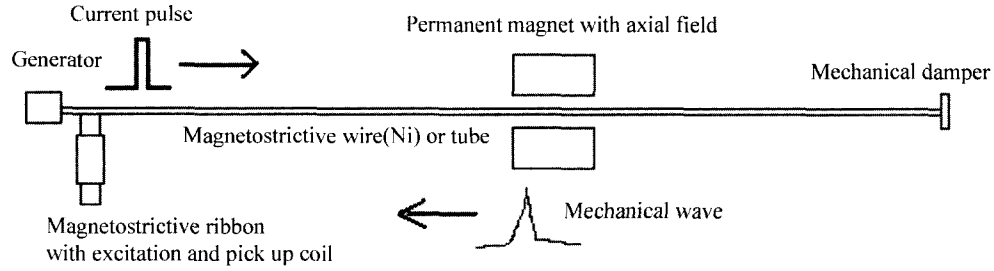

Fig. 5. Example of a position sensor based on the magnetostrictive properties of a Ni wire, excited by a current pulse producing a circular magnetizing field and a localized axial field produced by the permanent magnet at a certain position. The sum of the two excitations produces a mechanical twisting which propagates in the wire at the speed of sound allowing for the detection of the position of the magnet.

the pulse emission time and the mechanical wave arrival at the source end. At the other wire end there is usually a damper to absorb the mechanical wave and avoid echoes. The mechanical wave detector can be constructed with an amorphous ribbon which will change its permeability upon the arrival of the torsional wave, and a pick up coil. In some cases a piezoelectric material can also be used. Several position sensors of this type can be found on the market, with different spatial resolutions and for different maximum distances up to 50 meters with millimeter resolution see Figure 5.

Other types of displacement sensors are based on magnetostrictive delay lines, where a current pulse in a wire orthogonal to the magnetostrictive line generates a pulsed magnetic field and a coupled elastic wave in the line. Again the acoustic wave is propagated through the magnetostrictive delay line and detected by a receiving unit. In this case it is possible to detect the distance between the wire and the receiver. Several variations of this configuration are possible as discussed in [11-12].

7. Actuation with giant magnetostrictive and magnetic shape memory alloys

Magnetostrictive actuation is generally based on the Joule effect, describing the shape change of a sphere that becomes an ellipsoid upon application of a magnetic field, this effect is typically used in highly anisotropic geometry *i.e.* to produce a length change in a rod or radial vibrations of a ring composed by connected rods. Materials conventionally used for actuation are magnetostrictive elements like nickel, cobalt, iron, their alloys and also some Co based ferrites. These materials posses a magnetostriction typically lower than 1×10^{-4}. In recent years (1970-1980), after the discovery and development of Terfenol-D (bulk, laminations, powders) and other rare earth based materials with giant magnetostriction, up to 2.4×10^{-3} there has been an increasing number of applications based on magnetostrictive actuators. Magnetostrictive actuation with conventional materials competes directly with piezoelectric materials like barium titanate and lead zirconate titanate (PZT) while in the case of high power applications we can only use Terfenol-D.

In very recent times there has been the discovery of magnetic shape memory materials (Ni_2MnGa and FePd) which can reach a strain up to 6% due to a rearrangement of the martensite structure induced by a magnetic field. In spite of this wide variety of available materials it should be noted that pure Ni is still a material of choice in many applications, due both to the low cost and to the absence of aging processes which lead to the decay of properties in both Terfenol-D, shape memory and piezoelectric materials.

8. Magnetostrictive actuators

Several types of actuators have been developed using Terfenol-D a giant magnetostrictive alloy of composition $Tb_{0.3}Dy_{0.7}Fe_{1.92}$ (or its low temperature counterpart Terzinol $Tb_{0.3}Dy_{0.7}Zn_1$ with a maximum 0.5% strain) among which sonar, vibration dampers, fuel injectors, valve actuators, acoustic speakers etc. Unfortunately Terfenol-D is not very especially in the final form of oriented twinned single crystal of large dimensions, which is the only structure capable of achieving a maximum strain in the range of 2×10^{-3} or above (up to 2.4×10^{-3}). Commercial grade single crystals typically achieve a strain of 1.6×10^{-3} but due to price issues many applications rely on lower performance but cheaper crystals, polycrystals or bonded powders. The lower end materials, polymer bonded non-oriented powders, can still achieve a good 6.5×10^{-4} strain [11] at saturation and may be used for dynamic applications exceeding 10 kHz. It should be noted that, with respect to single crystals or polycrystals, this material requires a comparatively high applied field to achieve a given induction, due to the lower density and to the effect of demagnetizing fields on the composite powder. Composite powder samples are cheaper because they can be produced directly from milled polycrystals which are mixed with a polymer binder and compacted under high pressure. They can be magnetically aligned imposing a field during compaction, a treatment which enhances the maximum achievable strain.

In the typical actuator the Terfenol-D rod is enclosed in a cylindrical magnetic circuit which is designed to generate intense fields in the range of 100 kA/m, the rod, positioned on the cylinder axis and surrounded by a large solenoid, is pre-stressed in compression to achieve a maximum deformation at a given field. Additionally a bias field is applied through a permanent magnet to shift the zero current point to the region of maximum strain to field response. The application of a bias also avoids the typical frequency doubling of the mechanical output with respect to the magnetic field, due to the insensitivity of magnetostrictive strain to the field sign. Given the complexity of the magnetic circuit of the actuator we can understand that a detailed analysis of all the components is needed for the design of a working device, where the strain vs. field characteristic of the rod will only give us the material properties regardless of all other parameters of the magnetic and mechanical configuration which play a fundamental role to define the strain vs. applied field

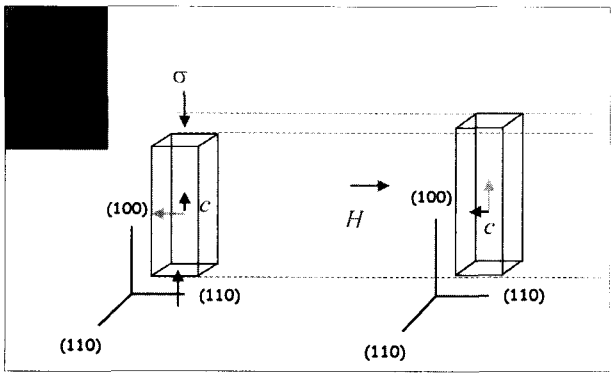

Fig. 6. An oriented single crystal sample of Ni_2MnGa is subjected to compressive stress in the low temperature martensite phase. As the sample contracts the tetragonal cells will preferably orient their "c" axes along with stress. A magnetic field can partly or fully reorient the "c" axis which is also the magnetic anisotropy axis. Regions with different orientations of the "c" axis are separated by twin boundaries which appear as lines at about 45° with respect to the sample edges -see inset-.

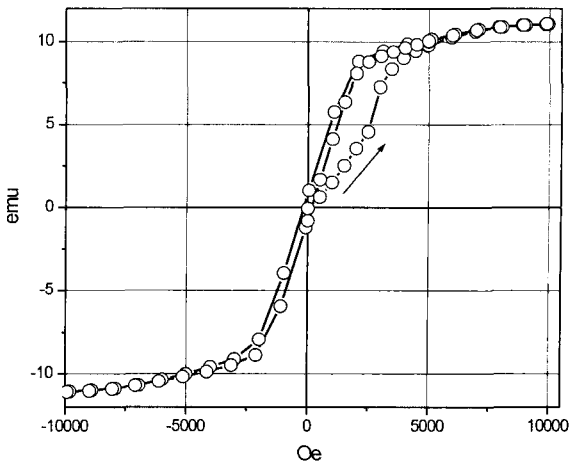

Fig. 7. Vibrating sample magnetometer loop of an oriented Ni_2MnGa single sample with 3.5% strain in the (100) direction. The measurement starts in the demagnetized state after a thermal sample reset. Upon magnetization a threshold field is reached and the sample strains due to the reorientation of the short "c" axis carrying the anisotropy. Subsequent magnetization along the same direction will not produce strain. Magnetization after a 90° sample rotation will again produce strain.

characteristics.

9. Magnetic shape memory actuators

Ni_2MnGa and $Fe_{70}Pd_{30}$ are the only alloys known to date to posses shape memory effects which can be excited through a magnetic field. In recent years most of the research has been devoted to the Ni_2MnGa system, which has shown a 6% strain in a field of about 300 kA/m, while the demonstrated output of the FePd system is about 1.2%. It is important to clarify that the phenomenology beneath this giant deformations is completely different from magnetostriction. Shape memory materials have two stable phases and in the case of Ni_2MnGa, which is the simpler system, the low temperature phase is martensitic with a tetragonal unit cell. The tetragonal cell has a shorter axis "*c*" which is also the magnetic anisotropy axis [14-17]. A large pseudo-plastic strain (up to 6%) is obtained when an oriented single crystal sample of Ni_2MnGa is subjected to compressive stress (in the range of 1-10 MPa) in the low temperature martensite phase. As the sample contracts the tetragonal cells will preferably orient their "*c*" axes in the direction of stress (see figure 6). The peculiarity of these materials is due to the correspondence of the "*c*" axis with an easy axis of magnetization. Given this property, a magnetic field may be able to reorient the tetragonal cells. This process requires a low energy if it is due to the motion of twin boundaries, which separate the regions of the sample with equally oriented unit cells. This process is similar to magnetization through domain wall motion, which is a lower energy process with respect to magnetization by rotation. Once Ni_2MnGa single crystals of proper composition (a little off stoichiometry) have been produced, oriented and cut the magnetic field is able to select and help the growth of variants of the martensite with the "*c*" axis pointing in the same direction. An increasing magnetic field will thus cause a growth of this type of variants through the motion of twin boundaries (the mechanical counterpart of 90° domain walls). If we measure a magnetization loop, the magnetization curve will present a discontinuity (see figure 7) when the threshold field required for reorientation of the "*c*" axis is reached. This means that the reorientation of the "*c*" axis will cause an irreversible giant strain, but also an irreversible change of the magnetic anisotropy of the samples. The behavior can be observed again after a rotation of 90° of the sample or after a heating above the martensite to austenite temperature.

It has been recently clarified that in these systems the magnetic field acts as an equivalent stress so that giant strain is obtained due to a particular mechanical softness or pseudo-plastic behavior, which is shown in the stress-strain curve (figure 8) where the mechanical yielding appears at a very low applied stress value. Depending on the single crystal composition, structure and also on external stress and temperature this threshold level can change, and may reach values too high to be achieved with the simple coupling between magnetic field and magnetic anisotropy.

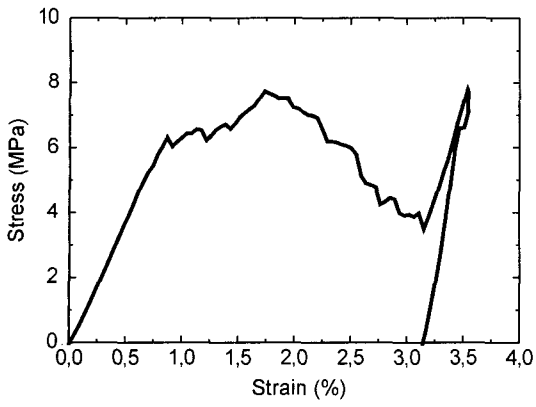

Fig. 8. [100] compressive stress *vs.* [100] strain curve of the slab ($1 \times 4 \times 5$ mm^3) sample, with all {100} faces and edges. For each measurement the sample is heated above T_A at 390 K, then cooled at 300 K, below T_M under a 0.3T [100] field (perpendicular to the measurement direction). The pseudo-plastic behavior shown in the stress-strain curve shows a mechanical yielding at a very low applied stress value. The yielding point may change depending on the single crystal composition, structure and also on external stress and temperature.

10. Modeling the behavior of magnetic shape memory actuators

In recent years several attempts have been made to describe, and possibly predict the magnetic and mechanical properties of Ni_2MnGa [18-20]. To address this issue here we compare the mechanical and magnetization experimental results obtained on two identical samples of Ni_2MnGa oriented single crystals with the predictions of a phenomenological model, in order to clarify and quantify the role of the occurring physical phenomena. The model is based on the assumption that the magneto-elastic interaction can be described as a stress acting on the crystalline lattice. This assumption allows to establish an equivalence between applied magnetic field and stress, mediated by the magneto-elastic constants of the material. This approach has been successfully used to describe the quasi reversible strain behavior of Ni_2MnGa alloys [21, 22]. Here the same approach is extended to analyze the large strains due to the irreversible motion of twin boundary interfaces under the pressure of the magnetic field. To this end a statistical distribution is assumed for the energy barriers hindering the growth of favorable martensite variants. The model parameters are derived from the experimental stress vs. strain and magnetization *vs.* field curves. The modeling procedure is validated by comparing the model predictions with the observed non linear mechanical and magnetic behavior of the material. In particular a theoretical value of the energy conversion coefficient is determined $c_{me}=1.57 \times 10^{-4}$ MPa $(kA/m)^{-2}$, in good agreement with the value $c_{me}=1.25 \times 10^{-4}$ MPa $(kA/m)^{-2}$ determined through the comparison of experimental stress-strain curves and magnetization curves.

11. Stress-magnetic field equivalence

A model for the equivalence between stress and applied magnetic field in a ferromagnetic martensite has also been discussed in a previous paper [22], here we report a brief summary. Starting from the expression of the Gibbs potential for a single magnetic domain cubic crystal one adds the distortion of the cubic cell consequent to the martensite phase transition to the magnetostrictive and stress induced strain. In the case of Ni_2MnGa, a cubic to tetragonal martensitic transformation with a negative magnetostriction constant occurs, and the deformation of the parent cell will produce a uniaxial anisotropy along the shorter c axis. One can extract the magnetoelastic energy term from the Gibbs energy potential obtaining

$$F_{me}=\delta M_S^2[\sqrt{3}(m_x^2-m_y^2)u_2+(2m_z^2-m_y^2-m_x^2)u_3]. \quad (1)$$

The differentiation of Eq. (1) with respect to strain defines a stress proportional to the square of the magnetization vector:

$$\sigma_2^{me}=6\sqrt{3}\,\delta M_S^2(m_x^2-m_y^2),\ \sigma_3^{me}=6\delta M_S^2(2m_z^2-m_y^2-m_x^2) \quad (2)$$

where $u_{1,2}$ are linear combinations of the strain tensor components, $m_{x,y,z}$ are the components of the unit magnetization vector, and δ is a phenomenological coupling constant. Under the action of an external magnetic field the rotation of the magnetization vector is accompanied by the appearance of the field-induced stress $\sigma_{2,3}(H)=\sigma_{2,3}^{me}(H)-\sigma_{2,3}^{me}(0)$. When the magnetic field is applied transversally to the easy magnetization axis of the variant, it induces a stress $\sigma(H)\equiv\sigma_2(H)/\sqrt{3}=A\cos^2\psi(H)$, where $A=-12\delta M_S^2$ and ψ is the angle between m and H. The $\cos\psi$ term linearly depends on the magnetic field, i.e. $\cos\psi=H/H_S$, when $H<H_S$ or 1, when $H\geq H_S$, where H_S is a constant magnetic field. According to the above expressions,

$$\sigma(H)=c_{me}H^2, \quad (3)$$

where $c_{me}=-12\delta M_S^2/H_S^2$.

12. Statistical model

The microstructure of a martensite deriving from a cubic structure can be modeled by considering the alternating variants of a tetragonal crystal lattice in twin

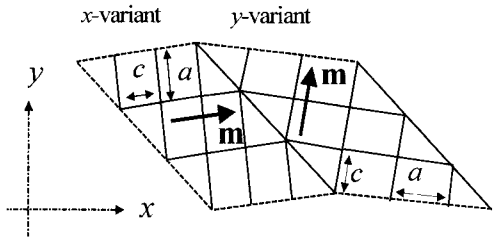

Fig. 9. Two variants in twin relation. The tetragonal crystalline structure in the two twinned variants is schematically represented. The magnetization vector inside each variant is aligned to the short edge (c) of the cell that represents an easy magnetization direction. The two variants are separated by a twin boundary. c and a are constant on both sides of the boundary.

relation. The orientation of the x and y axes is chosen close to that of the c-axes in the twinned variants (an example of xy-structure is shown in Fig. 9). Assuming that the magnetic field H is applied along the y direction, the magnetic and magnetoelastic responses of a martensite in the xy-structure can be modeled under the following assumptions [23]:

The rearrangement of xy-twins under an increasing stress $\sigma(H)$ occurs in two stages:

– a reversible displacement of the twin boundary is coupled to the partial rotation of the magnetic vector of the x-variant from the x direction toward the y direction;

– once a critical stress-field value is reached the twin boundary jumps irreversibly, the x-variant disappears and the magnetic vector becomes aligned to the y direction all over the spatial domain previously occupied by the twin.

The critical field values H_n and the relative threshold stress values $\sigma_n=\sigma(H_n)$, coupled to the jumps of the twin boundaries, are different for the different twins.

The critical stress values σ_n are distributed around the average value σ_c and their distribution is Gaussian:

$$p_n=\frac{1}{Z}\exp\left\{-\frac{(|\sigma_n|-|\sigma_c|)^2}{2\sigma_0^2}\right\},\quad Z=\sum_n \exp\left\{-\frac{(|\sigma_n|-|\sigma_c|)^2}{2\sigma_0^2}\right\}, \tag{7}$$

where σ_0 is a constant parameter.

The jump of each twin boundary is accompanied by the abrupt alignment of the c-axis of the x-variant to the direction of the field H. The number N of "relaxed" twins can be found from the condition $|\sigma(H)| \geq |\sigma_n|$, which results in the expression

$$N(\sigma)=N_0\sum_n p_n\theta(|\sigma|-|\sigma_n|), \tag{8}$$

where N_0 is the initial number of twins, θ is the Heaviside function and $\sigma \equiv \sigma(H)$

The same approach can be used for the description of magnetization loops. The volume fraction of the y-variant in the xy-structure, affected by the increasing stress $\sigma(H)$, satisfies the equations

$$\alpha_y(\sigma)=\begin{cases}\alpha_y(0)[1-N(\sigma)/N_0], & \sigma<0,\\ \alpha_y(0)+[1-\alpha_y(0)]N(\sigma)/N_0, & \sigma\geq 0.\end{cases} \tag{9}$$

For the reverse stress path we have

$$\alpha_y(\sigma)=\begin{cases}\alpha_y(\sigma_{\max})[1-N(\sigma)/N_0], & \sigma<0,\\ \alpha_y(\sigma_{\max}), & \sigma\geq 0.\end{cases} \tag{10}$$

where $\sigma_{\max}$ is the maximal stress value achieved during the forward field path.

The equations for the field-induced strain are:

$$\varepsilon_{xx}(H)=(S^{-1}/2)\sigma-(c/a-1)[\alpha_y(\sigma)-\alpha_y(0)],$$
$$\varepsilon_{yy}(H)=-S^{-1}\sigma+(c/a-1)[\alpha_y(\sigma)-\alpha_y(0)],$$
$$\varepsilon_{zz}(H)=(S^{-1}/2)\sigma, \tag{11}$$

where a and c are the values of lattice parameters in the martensitic phase and S is the stiffness coefficient. Equations. (10) and (11) are obtained for the case $c/a<1$. They describe field-induced strains and the stressstrain relations obtained during the mechanical testing (see Fig. 9). The terms containing the stiffness coefficient S correspond to reversible strain contributions whereas the terms containing volume fractions of the variants α correspond to irreversible strains [23]. As a first approximation we also assume that magnetization processes here involve: (a) the reversible rotation of the magnetic vectors of the variants; (b) a reversible displacement of the 180° magnetic domain walls; (c) the irreversible reorientation of martensite variants (field-induced stress relaxation) which are expressed by the following terms:

$$M_{\text{rot}}=M_S[(H/H_S)\theta(H_S-H)+\theta(H-H_S)],$$
$$M_{\text{dis}}=M_S[(H/H_c)\theta(H_c-H)+\theta(H-H_c)],$$
$$M_{\text{rel}}=\alpha_y(H)M_{\text{dis}}+[1-\alpha_y(H)]M_{\text{rot}}, \tag{12}$$

where H_c is the critical field for the disappearance of the 180° domain walls structure. M_{rot} and M_{dis} are derived taking into account magnetic saturation [23], while the term M_{rel} takes into account how the magnetization is coupled to stress and causes irreversible structural rearrangements accounted by the α volume fraction (see Eqs. 8-10). M_{rel} is expressed for the case of large area martensite variants (twins) which can include a few magnetic domains separated by 180° domain walls. In such a case the stress relaxation in the xy-structure is accompanied by both the rotation of the magnetic vector (for x-variants)

and the displacement of magnetic domain walls (for *y*-variants). Since it can be expected that the *xy*-, *zy*- and *zx*-structures initially arise in equal amounts in the specimen, $\langle M\rangle = 1/3(M^{xy} + M^{zy} + M^{zx})$, where M^{ij} is the magnetization of the spatial domain of martensite initially occupied by the *ij*-structure. For the first forward path of the field H_y we can assume that $M^{xy}=M^{zy}=M_{rel}$, $M^{zx}=M_{rot}$. Different initial states of the sample can be accounted by a proper choice of the $\alpha_y(0)$ value without any changes in the expressions of M_{rel} above. Taking into account the irreversible character of the stress relaxation (corresponding to a reorientation of the martensite) and the 180° magnetic domain wall structure, for the reverse field path and all further paths we obtain $M^{xy}=M^{zy}=M_{dis}$, $M^{zx}=M_{rot}$. Using Eqs. (7)-(10), and the previous expressions of M we are thus able to compute the magnetization loops for single crystals in martensitic state.

13. Experimental results and discussion

One cube and one slab sample were cut from a $Ni_{51.0}Mn_{27.9}Ga_{21.1}$ oriented single crystal grown by induction method at the Swiss Federal Institute of Technology (ETH) Zürich. The crystal was annealed at 900°C for 40 h under an *Ar* atmosphere. The samples are characterized by a $T_M = 314$ K, $T_A = 316$ K, $T_C = 370$ K where T_M and T_A are the forward and reverse martensitic transformation temperatures respectively and T_C is the Curie temperature, measured by low field magnetic susceptibility. Mechanical and magnetization experimental data were used to determine the parameters of the distribution of energy barriers and the conversion factor c_{me} connecting the induced stress to the magnetic field. Prior to either magnetic or mechanical tests the initial state of the sample was forced to single variant (*x-variant*) by cooling from the austenite phase to 300 K under a 0.3 T magnetic field. Stress-strain curves were measured on the sample with a slab geometry (5 mm × 4 mm × 1 mm) by means of a microprocessor controlled mechanical test system. As shown in Fig. 8 the *stress-strain* curve exhibits an initial linear portion at low *stress* (below 5 MPa) where the elastic stiffness of the material is predominant and no irreversible twin boundary displacement occurs. The onset of a twin boundary displacement processes occurs around 5 MPa, causing a large irreversible strain after which another elastic region is reached. The cubic sample (2.6 mm long edge) with (100) faces was magnetically characterized by VSM magnetometry measurements. After cooling under a 0.3 T field along the <100> direction, the sample was magnetized along one of the orthogonal [100] directions. An irreversible jump of the magnetic susceptibility is observed during the first field ramp (Fig. 7, dots-thin line), accompanied by a large magneto-strain driven by the twin boundary motion. In the framework of the present statistical model, the value of field at the susceptibility jump and the yield stress shown in Fig. 8 must be consistent with Eq. (3). This comparison gives an experimental conversion factor of $c_{me}=1.25 \times 10^{-4}$ MPa $(kA/m)^{-2}$. The theoretical curve shown in Fig. 10 line, superimposed to the one in Fig. 7 open dots-line was computed from the Eqs. (7)-(10) and the expressions of M appearing in section 12. In particular a tetragonal martensite cell with lattice parameters $a = b = 0.591$ nm and $c = 0.558$ nm was used, a field $H_S = 640$ kA/m (see for example [22]) and a saturation magnetization $M_s = 0.57$ T was derived from the measured magnetization curves. In accordance with the experimental procedure the sample is assumed in an initial *x*-variant state with $\alpha_y(0)=0$. A good fit of the experimental magnetization curves is obtained in Fig. 10 using the following assumptions and parameters: a Gaussian distribution of energy barriers with a mean $\sigma_c = 0.95$ MPa and a standard deviation $\sigma_0=\sigma_c/4$, a phenomenological coefficient $\delta = -23$ Mpa T^{-2}. Using these parameters one can obtain a theoretical value for the conversion coefficient of $c_{me} = 1.57 \times 10^{-4}$ MPa/kA^2m^{-2}. This result is in good agreement with the experimentally determined value of 1.25×10^{-4} MPa $(kA/m)^{-2}$. Therefore on the basis of a statistical model, assuming an equivalence between the applied magnetic field and a magnetically induced stress it is possible to evaluate the critical stress that is necessary to overcome twin boundary pinning in a defined martensite structure.

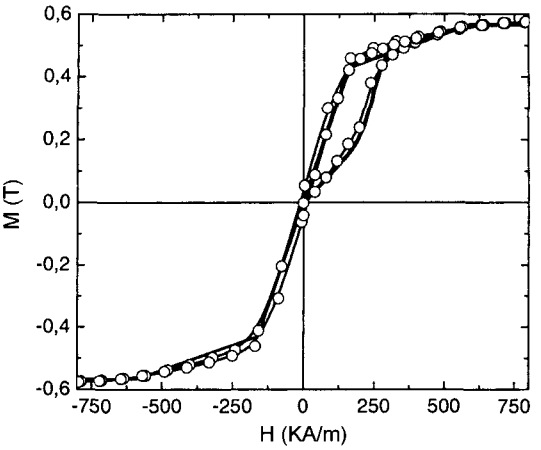

Fig. 10. Experimental VSM (dots-thin line) and modeled (thick line) magnetization curve. A low susceptibility is observed when the sample is first magnetized. Around 200 kA/m an abrupt change of the susceptibility is observed due to the rearrangement of the easy axis which accompanies a large strain.

Summary

We have presented a review of mechanical sensing techniques based on magnetic methods, in particular magnetoelastic strain gauges and force sensors were discussed. We described a novel strain sensor constructed with soft amorphous ribbons possessing a small negative magnetostriction. A review of magnetic actuators based on giant magnetostrictive materials was shown. Recent advances in the development and application of magnetic shape memory materials were also discussed, coupled to an analysis of recent studies for the description of magnetic shape memory phenomena, where an equivalence between field and stress was presented.

References

[1] M. Pasquale, A. Infortuna, L. Martino, C. Sasso, C. Beatrice, and S. H. Lim, Magnetic properties of TbFe thin films under applied stress, JMMM **215-216**, 769-771 (2000).
[2] J. Huang, C. Prados, J. E. Evetts, and A. Hernando, Phys. Rev. B, **51**(1), 297-304 (1995).
[3] Y. Hayashi, T. Honda, K. I. Arai, K. Ishiyama, and M. Yamaguchi, IEEE Trans. Mag. **29**(6), 3129-3131 (1993).
[4] Y. S. Choi, S. R. Lee, S. H. Han, H. J. Kim, and S. H. Lim, J.of All.and Comp. **258**, 155-162 (1997).
[5] D. K. Kleinke and H. M. Uras, Rev. Sci. Instrum **65**(5), 699-1710 (1994).
[6] W. Fleming, IEEE Trans. Veh. Tech. **38**, 159-167 (1989).
[7] I. Sasada, N. Suzuki, T. Sasaoka, and K. Toda, IEEE Trans Mag. **30**, 4632-4634 (1994).
[8] D. Son and J. Sievert, IEEE Trans. Mag. **26**, 2017-2019 (1990).
[9] I. J. Garshelis and C. R. Conto, IEEE Trans. Mag. **30**, 4629-4631 (1994).
[10] D. Son, S. J. Lim, and C. S. Kim, IEEE Trans. Mag. **28**, 2205-2207 (1992).
[11] E. Hristoforou and R. E. Reilly, IEEE Trans. Mag. **26**, 1563-1565 (1990).
[12] E. Hristoforou and R. E. Reilly, IEEE Trans. Mag. **30**, 2728-2730 (1994).
[13] M. Pasquale, C. Sasso, and S. H. Lim, IEEE Trans. Mag. **35**, 3829-3831 (1999).
[14] V. A. Chernenko, E. Cesari, V. V. Kokorin, and I. N. Vitenko, Scr. Met. Mat. **33**, 1239-1244 (1995).
[15] R. Tickle and R. D. James, J. Magn. Magn. Mat. **195**, 627 (1999).
[16] S. J. Murray, M. Marioni, S. M. Allen, R. C. O'Handley, and T. A. Lograsso, Appl. Phys. Lett. **77**(6), 886-888 (2000).
[17] O. Heczko, A. Sozinov, and K. Ullakko, IEEE Trans. Mag. **36**(5), 3266-3268 (2000).
[18] K. Ullakko, J. K. Huang, J. Kantner, V. V. Kokorin, and R. C. O'Handley, Appl. Phys. Lett. **69**, 1966 (1996).
[19] V. A. Chernenko, V. A. L'vov, M. Pasquale, S. Besseghini, C. P. Sasso, and D. A. Polenur, Int. J. Appl. Electromagnetics and Mechanics **12**, 3 (2000).
[20] S. J. Murray, M. Marioni, S. M. Allen, R. C. O'Handley, and T. A. Lograsso, Appl. Phys. Lett. **77**, 886 (2000).
[21] E. V. Gomonaj and V. A. L'vov, Magnetostriction of NiMnGa martensites, Met. Phys. Adv. Technol. **20**(9), 22 (1998).
[22] V. A., L'vov, S. P. Zagorodnyuk, and V. A. Chernenko, Eur. Phys. J. B **27**, 55 (2002).
[23] N. I. Glavatska, A. A. Rudenko, I. N. Glavatskiy, and V. A. L'vov, (submitted to JMMM).
[24] Massimo Pasquale, Carlo Paolo Sasso, Stefano Besseghini, Elena Villa, Thomas A. Lograsso, and Deborah L. Schlegel, IEEE Trans. Mag. **38**, 2847 (2002).
[25] O. Heczko and K. Ullakko, IEEE Trans. Magn. **37**, 2672 (2001).